Analysis of the 13-14 July Gulf Surge Event

During the 2004 North American Monsoon Experiment

Peter J. Rogers[1] and Richard H. Johnson

Department of Atmospheric Science

Colorado State University

Fort Collins, CO 80523

April 2006

(submitted to *Mon. Wea. Rev.*)

[1] *Corresponding author address:* Peter J. Rogers, Department of Atmospheric Science, Colorado State University, Fort Collins, CO 80523. E-mail: progers@atmos.colostate.edu

Abstract

Gulf surges are disturbances that move northward along the Gulf of California (GoC), frequently advecting cool, moist air from the GoC or eastern tropical Pacific Ocean into the deserts of the southwest United States and northwest Mexico during the North American Monsoon (NAM). Little attention has been given to the dynamics of these disturbances due to the lack of reliable high-resolution data across the NAM region. High temporal and spatial observations collected during the 2004 North American Monsoon Experiment (NAME) are used to investigate the structure and dynamical mechanisms of a significant gulf surge on 13-14 July 2004. Integrated Sounding Systems (ISSs) deployed along the east coast of the GoC and an enhanced network of rawinsonde sites across the NAM region are used in this study.

Observations show that the 13-14 July gulf surge occurred in two primary stages. The first was preceded by anomalous warming and a low-level nocturnal inversion along the northern GoC on 13 July. Sharp cooling, moistening, and increased low-level south-southeasterly flow followed over a 12-18 h period. Over the northern gulf, winds reached ~20 m s^{-1} at 750 m above sea level. Then there was a brief respite followed by the second stage - a similar, but deeper acceleration of the southerly flow in association with the passage of Tropical Storm (TS) Blas on 14 July. The initial surge disturbance traversed the GoC at a speed of ~17-22 m s^{-1} and resulted in a deepening of the mixed layer along the northern gulf. Dramatic surface pressure rises also accompanied the surge.

The weight of the evidence suggests that the first stage of the overall surge consisted itself of two parts. The initial part had characteristics of bore-like disturbances initiated by convective downdrafts impinging on the nocturnal inversions over the region. The secondary part was characteristic of a Kelvin wave-type disturbance, as evident in the deeper layer of sharp cooling

and strong winds that ensued. Another possible explanation for the first part is that the leading edge of this Kelvin wave steepened nonlinearly into a bore-like disturbance. The data are not adequate to delineate between these possible mechanisms. The second stage of the surge was associated with the increased circulation around TS Blas.

1. Introduction

The North American Monsoon (NAM) is an atmospheric circulation phenomenon characterized by an increase in convective activity and precipitation, beginning in early July and continuing through mid-September across northwest Mexico and the southwest United States (Bryson and Lowry 1955; Douglas et al. 1993; and Adams and Comrie 1997). Monsoon onset was originally attributed to the westward extension of the southeast United States subtropical high (Jurwitz 1953; Bryson and Lowry 1955; and Sellers and Hill 1974), resulting in a mid-tropospheric wind shift from dry westerlies to moist southeasterlies. However, the source of moisture associated with monsoon onset along the Gulf of California (GoC) and into Arizona remained unclear (Reitan 1957; Rasmusson 1967). In particular, if the source was from the Gulf of Mexico, how could water vapor from there traverse up and over the Sierra Madre Occidental (SMO) and end up in the GoC given the large altitude and extent of this mountain barrier? A partial resolution of this issue came about through the studies of Hales (1972) and Brenner (1974), who introduced the moisture "gulf" surge (hereafter gulf surge) as a mechanism for transporting low-level cool, moist air northward along the GoC during the NAM.

Noting the orographic features surrounding the GoC (Peninsular Range to the west and SMO to the east) (Fig. 1), Hales (1972) suggested that a natural channel exists for gulf surge propagation. Due to decreased frictional effects over water, gulf surges are strongest over the GoC and follow the path of least resistance, thus continuing most forcefully up the Colorado

River Basin upon reaching the northernmost extent of the GoC (Hales 1972; Brenner 1974). Hales (1972) found that a gulf surge on 1-2 September 1970 traversed the entire length of the gulf at a speed of ~15 m s^{-1}. Simulations of gulf surges by Stensrud et al. (1997) found speeds over a wide range of 10-23 m s^{-1}.

Through a series of case studies, Hales (1972) and Brenner (1974) noted several common characteristics of gulf surges (Fuller and Stensrud 2000): 1) gulf surge onset is accompanied by a significant drop in surface temperature, increases in sea-level pressure and surface dewpoint temperature (relative humidity), a surface wind shift with an increased southerly component, and increased low-level cloudiness, 2) gulf surge-related cooling and moistening are greatest above the surface and decrease in strength with height, 3) gulf surges are strongest at their onset, but decrease in intensity once having fanned out over the low deserts of Arizona, and 4) deep gulf surges result in increased convective development across much of Arizona. The kinematic and thermodynamic characteristics of gulf surges were further elucidated in a sounding composite study by Douglas and Leal (2003).

Hales (1972) and Brenner (1974) also noted relationships between large cloud masses over the central and/or southern GoC and subsequent surges of moisture, implying a disturbance in the low-level pressure balance along the GoC. Strengthening domes of higher pressure related to "convective activity, evaporational cooling from precipitation, and differential heating in and outside the cloud" were suggested as mechanisms for such a disturbance (Hales 1972). The amplification of the along-gulf pressure gradient thus provides the impetus necessary to transport moisture northward (Hales 1972; Brenner 1974). Several studies have since linked the development of these large cloud masses with westward-moving hurricanes, tropical cyclones, or mid-tropospheric easterly waves (Stensrud et al. 1997; Fuller and Stensrud 2000; and Douglas

and Leal 2003). Others have suggested connections with upper-tropospheric inverted troughs (Pytlak et al. 2005) or mesoscale convective systems (MCSs) that develop along the SMO and GoC coastal plain (Adams and Comrie 1997).

The dynamical mechanisms by which gulf surges propagate northward along the GoC have received little attention in the literature, especially from an observational standpoint. Most likely this is a consequence of little reliable high-resolution data across the NAM region except for brief periods during the Southwest Area Monsoon Project (SWAMP) in 1990 (Douglas 1995) and 1993 (Douglas and Li 1996). Zehnder (2004) investigated four possible linear gulf surge dynamical mechanisms: gravity currents, ageostrophic isallobaric flow, Rossby edge waves, and barrier Kelvin waves. He concluded that Rossby or Kelvin wave dynamics may be the most likely explanation for this phenomenon. However, nonlinear dynamical mechanisms or a combination of those discussed by Zehnder (2004) may also be linked to gulf surge propagation.

Zehnder (2004) noted that detailed observations are needed to confirm or refute various theories of the dynamics of gulf surges. Therefore, the primary objective of this study is to use high-resolution data collected during the 2004 North American Monsoon Experiment (NAME) to describe in unprecedented detail the structure of the significant gulf surge event on 13-14 July 2004, and attempt to understand its dynamical mechanisms.

The remainder of this paper is structured as follows. Section 2 will describe the NAME field campaign and the data used for this study. Section 3 will detail the synoptic and convective environments surrounding the gulf surge event. Section 4 will examine the gulf surge vertical and horizontal structures. Section 5 will describe the propagation characteristics of the gulf surge, as well as suggest a possible dynamical mechanism for propagation. Finally, Section 6 will provide a brief summary and conclusions.

2. Data and Methods

a.) NAME Structure and Gulf Surge Identification

The NAME extended observing period (EOP) was conducted from 1 June to 30 September 2004, although many instrumentation platforms were only in operation from 1 July to 15 August. During this latter period, there were nine intensive observing periods (IOPs) involving 18 IOP days. IOPs were generally accompanied by an increased frequency of rawinsonde launches from the sounding network (Fig. 1) and National Oceanic and Atmospheric Administration (NOAA) WP-3D aircraft flights in the vicinity of the GoC.

The gulf surge investigated in this study occurred on 13-14 July during IOP 2 (Higgins et al. 2006). To capture pre- and post-surge conditions, the period of interest examined for this event was 0000 UTC 11 July to 0000 UTC 16 July. Several other surges were observed from 1 July to 15 August, but the 13-14 July case was one of only two major events during NAME, the other occurring on 22-24 July.

b.) Integrated Sounding System

Maintained by the National Center for Atmospheric Research (NCAR), three Integrated Sounding Systems (ISSs) (located at Puerto Peñasco and Bahia Kino in Sonora, and Los Mochis in Sinaloa) were deployed from 7 July to 15 August (Fig. 1). The ISSs consisted of 1) a global positioning system (GPS) balloon-borne atmospheric rawinsonde system, which measured pressure, temperature, relative humidity, and wind speed/direction at one-second resolution, 2) a 915 MHz Doppler clear-air wind profiling radar (profiler hereafter), which measured wind speed and direction (~100 m vertical resolution) up to several kilometers AGL at half-hour intervals, 3) an enhanced surface observing station, which measured surface pressure, temperature, relative humidity, wind speed/direction, radiation, and precipitation at one-minute resolution, and 4) a

Radio Acoustic Sounding System (RASS), which measured vertical profiles of virtual temperature at half-hour intervals. Due to the proximity of the ISS sites at Puerto Peñasco and Bahia Kino to the local populace and the unpleasant sound which the RASS emits, operators shut down the system at night (~2200 to 0800 LT) at these sites. Unfortunately, initial gulf surge passage occurred in the early morning and was not observed by the RASS along the northern GoC. Therefore, RASS data were not used in this study.

ISS sounding data were run through the NCAR-developed Atmospheric Sounding Processing Environment (ASPEN) quality control program, which smoothed the profiles and removed suspicious data points. Additional quality control was later conducted that included visual checks and profile comparisons to check for major discrepancies (W. Brown 2004, personal communication). The NCAR Improved Moments Algorithm (NIMA) quality control program was used to correct bad or questionable profiler data. In addition, only those data with confidence values greater than 0.5, as calculated using the NCAR Winds and Confidence Algorithm (NWCA), were considered reliable (W. Brown 2004, personal communication). In constructing wind profiler plots, surface data were added from the surface meteorological stations since the first profiler range gate was ~120-180 m AGL. The quality of the data collected at the surface stations was excellent, thus requiring no significant quality control effort.

c.) NAME Rawinsondes and Observational Gridded Analyses

An extensive rawinsonde network (Fig. 1) was deployed during the NAME EOP. In the region from 15°-40°N and 90°-120°W, the National Weather Service (NWS) supported 23 sites, 10 of which launched four rawinsondes per day during the IOPs, while the Servicio Meteorológico Nacional (SMN - Mexican Weather Service) supported 13 sites, five (two) of which launched six (four) rawinsondes per day during the IOPs. Other sites with high temporal

frequency rawinsonde launches with varying schedules included the Research Vessel (RV) *Altair* at the mouth of the GoC (23.5°N, 108°W), Loreto, Baja California Sur, Yuma, AZ, and Edwards Air Force Base (AFB), CA.

All NAME sounding data, including those from the ISS sites were processed through additional quality control procedures that mimicked those used during the Tropical Ocean Global Atmosphere Coupled Ocean Atmosphere Response Experiment (TOGA COARE) (Loehrer et al. 1996). These procedures included the computation of statistical means and standard deviations to check gross limits, objectively flagging data as questionable or bad, linear interpolation over missing data gaps, and visual inspection.

The quality controlled data collected from all rawinsonde sites were objectively analyzed using a multiquadric interpolation (Nuss and Titley 1994) onto a 1°x1° grid over 15°-40°N and 90°-120°W (Tier 2 Array - T2A) two times per day (0000 and 12000 UTC), and over 22°-35°N and 100°-115°W (Tier 1 Array - T1A) four times per day (0000, 0600, 1200, and 1800 UTC) with 25 hPa vertical resolution (surface, 1000 hPa - 50 hPa) (Johnson et al. 2006) (Fig. 1). In addition, profiler data from the ISS sites were included in the gridded analyses at those times where rawinsonde winds were unavailable. National Centers for Environmental Prediction (NCEP) reanalyses data (Kalnay et al. 1996) were used over data-sparse regions of the east Pacific Ocean and Caribbean Sea to assist the analysis.

d.) Additional datasets

Surface pressure data from numerous sites that report hourly observations in the standard World Meteorological Organization (WMO) METAR format were used in conjunction with ISS surface data to investigate surface pressure patterns associated with the surge event. Due to the lack of observations over Baja California, data were used from the SMN ten-minute automated

surface observing network to improve coverage over the peninsula. However, the overall quality of surface pressure data at the SMN sites (both WMO and automated) were quite poor and included unrealistic high frequency noise. An objective scheme was developed to remove the most obvious surface pressure errors, which was applied to all sites. Values greater than four standard deviations from the site's 7 July to 14 August mean were set to missing. Missing data gaps less than or equal to six hours were then filled by linear interpolation.

In addition, Geostationary Operational Environmental Satellite (GOES)-10 infrared (IR) images centered about the core monsoon region were obtained from the Cooperative Institute for Research in the Atmosphere (CIRA) to determine areas of relative cloudiness and convective activity associated with gulf surge initiation, propagation, and passage.

3. Large-Scale Environment

a.) Synoptic Conditions

Figure 2 highlights the T2A 700 and 200 hPa heights and wind vectors at 1200 UTC from 12 to 14 July, where 13 July is defined as the day of initial surge passage. At 700 hPa (Fig. 2a), two significant transient features are evident: a northwestward-expanding subtropical high and the northwestward propagation of Tropical Storm (TS) Blas. At 200 hPa (Fig. 2b), an upper-tropospheric inverted trough can be seen propagating south and west of the subtropical high.

The subtropical high's 700 hPa center of circulation on 12 July was located over the Texas-Louisiana gulf coast. By 14 July, the high's center broadened and anticyclonic flow stretched from Louisiana westward into Arizona and northwest Mexico. Cyclonic flow associated with TS Blas at 700 hPa is visible south of 20°N, 110°W on 12 July. The location, movement, and timing of this system are consistent with the interpretations of Fuller and Stensrud (2000) and Douglas and Leal (2003), who have related gulf surge initiation with easterly wave or tropical

cyclone passage south of the GoC. Higgins et al. (2005) have also shown that surges associated with tropical cyclones are often deeper and more intense than those that are not linked to tropical cyclone propagation. The northwestward propagation of TS Blas resulted in its center of circulation being south and west of the southern tip of Baja California on 13 July, and out over the open waters of the eastern Pacific Ocean by 14 July. The combined movements of TS Blas and the subtropical high generated strong southeasterly winds south of the mouth of the GoC on 13 July and over much of the GoC by 14 July.

At 200 hPa, a strong north-south oriented inverted trough (evident at this stage as a closed low) over north central Mexico was embedded within the subtropical high on 12 July. Also visible at 500 hPa (not shown) albeit much weaker, this feature appeared to originate over southeast Texas four days earlier (Pytlak et al. 2005). As the trough propagated west-northwestward, it substantially weakened such that by 13 July it was no longer discernable (Fig. 2b). In fact, water vapor imagery examined by Pytlak et al. 2005 suggests that the trough appeared to dissipate along the international border on 13 July.

b.) Convective Conditions

Figure 3 shows GOES-10 IR satellite images centered about the core NAM region on 13 July every six hours. At 2346 UTC (~1800 LT) 12 July (Fig. 3a), the northernmost extent of TS Blas was just south of the mouth of the GoC. A large thunderstorm complex was positioned over northern Sonora and southeast Arizona. Numerous convective cells developed along the SMO, perhaps in connection with various mesoscale processes, such as land/sea interactions, mountain-valley circulations, and/or convective instability as argued by Howard and Maddox (1988). It is possible that upper-level divergence associated with the inverted trough may have also aided in the convective development along the SMO (Pytlak et al. 2005).

Six hours later (Fig. 3b) TS Blas was farther north and its outer rain bands penetrated the southern GoC and Baja Peninsula. The convective cells over the SMO merged with the thunderstorm complex over northern Sonora to form an impressive MCS over the central and southern GoC coastal plain. Gulf surge initiation and propagation is most likely tied with this convective evolution along the coastal plain as well as the northwest propagation of TS Blas. However, by 1200 UTC (~0600 LT) 13 July (Fig. 3c), the MCS dissipated over the central GoC as TS Blas continued its track south and west of the tip of Baja California.

By the afternoon (1800 UTC) of 13 July (Fig. 3d), the convective environment over the northern and central GoC was suppressed, although TS Blas' center of circulation was now clearly visible to the southwest of Baja California. On the day after initial surge passage (14 July) the rain bands from TS Blas spread over the GoC region, while a large MCS developed over the low deserts of Arizona (not shown). The development of this MCS is related to the northward transport of moisture by the gulf surge (McCollum et al. 1995) and aided by the mid-tropospheric synoptic regime (Higgins et al. 2004).

4. Gulf Surge Structure

a.) Vertical Structure as Observed by ISS Profilers

Heretofore, Douglas and Leal (2003) have conducted the most comprehensive analysis of gulf surge vertical structure and evolution using 12-h rawinsonde data at Empalme over nine years. However, the NAME ISSs provide a much higher spatial and temporal resolution of this phenomenon (~100 m, half-hour). In this section wind profiler data, along with the surface observations, are presented at the ISS sites up to 2 km AGL for the period 12-14 July.

The arrival of gulf surge onset at Puerto Peñasco (Fig. 4a) was complicated by two convective outflows that preceded the surge-related wind maxima centered about 1400 UTC 13 July. The

first occurred at ~0000 UTC 13 July, as evident in a strong wind shift from southwest to southeast, with maximum speeds between 8 and 12 m s^{-1} up to 1.0 km. The second occurred at ~0400 UTC 13 July, with maximum speeds approaching 12 m s^{-1} near 500 m AGL by 0500 UTC. The strongest acceleration of the flow associated with the gulf surge itself occurred at ~1000 UTC 13 July with winds from the south-southeast at speeds between 8 and 12 m s^{-1} centered about 750 m AGL. Gradual intensification and deepening of this feature occurred, such that by 1400 UTC, maximum speeds approached 20 m s^{-1} from the south-southeast centered near 700-800 m and the surge extended vertically to near 2.0 km. The strength and location of the peak winds over the northern GoC are in good agreement with NOAA WP-3D wind measurements obtained from a saw-tooth flight pattern on the afternoon of 13 July (not shown) and are also in good agreement with previous SWAMP flights (Douglas 1995; Stensrud et al. 1997). It is important to note that the peak winds in the surge were at a higher level (~750 m) than the convective outflows, which at this and other times were observed to be between 300 and 500 m. The latter features are gravity-current-driven phenomena and are expected to occur over a shallow layer (Wakimoto 1982).

The surface wind did not respond as dramatically to surge onset, although there was a slight strengthening and turning of the flow to the southeast. The most intense winds aloft significantly weakened by 0000 UTC 14 July. In addition, relatively strong flow occurred throughout most of 14 July below ~1.25 km with maximum speeds from the southeast as high as 16 m s^{-1}. This pattern does not appear to be a continuation of the prior day's initial gulf surge. Rather, Figs. 2a and 3 suggest it is likely due to the northwest propagation of TS Blas.

The most notable surface feature of the surge passage was a sharp pressure rise early on 13 July (Fig. 4b), followed by a continued overall increase of ~8 hPa over a two-day period. There

was also evidence of surface cooling on 13 and 14 July, and a very slight decrease in the dewpoint temperature during the surge period. The latter behavior contrasts with the dramatic dewpoint increase from 0000 to 1700 UTC 13 July (~12 ºC) that occurred at Yuma accompanying this surge, a phenomenon that has often been used to identify surge arrival in Arizona (Stensrud et al. 1997; Fuller and Stensrud 2000). The implications of these surface features will be discussed later[1].

Whereas gulf surge onset at Puerto Peñasco was preceded by convective outflows, surge onset at Bahia Kino appeared abruptly at 0600 UTC 13 July (Fig. 5a). There was an acceleration of the flow up to nearly 2.0 km with peak winds approaching 20 m s^{-1} from the south-southeast near 1.25 km by 1000 UTC on the 13 July. Overall, the maximum winds were at a slightly higher level than those at Puerto Peñasco. Again, surface winds were not significantly affected by surge passage, with only a slight strengthening and turning of the flow to the southeast. The gulf surge also quickly weakened and appeared to be disconnected from the relatively strong south-southeasterlies on 14 July associated with TS Blas. Similar to Puerto Peñasco, there was a sharp pressure rise of ~9 hPa over a two-day period, a slight temperature drop, but very little change in the dewpoint temperature (Fig. 5b).

The character of the surge at Los Mochis (Fig. 6a) is somewhat different from its appearance at Puerto Peñasco and Bahia Kino. Two convective outflows passed the site. The first occurred at ~1600 UTC 12 July, with maximum southeasterly flow of ~10 m s^{-1} at 300 m AGL. The second (near 0400 UTC 13 July) was embedded within an overall increase in the wind speeds starting around 0000 UTC. The period of stronger winds below 2.0 km from ~0000 to 1200 UTC 13 July appears to be the signal of the surge at Los Mochis. If so, it is weaker over the

[1] The surface traces presented in Figs. 4a, 5a, and 6a include tidal effects, whereas those in Fig. 11 do not. Therefore, surge-related surface pressure and temperature changes are best depicted in Fig. 11.

southern GoC although occurring at an earlier time. However, the Los Mochis site was ~10 km inland and therefore may not have accurately sampled the true strength of the surge as it passed over the GoC (Higgins et al. 2006).

NOAA WP-3D aircraft measurements during a flight along the GoC suggested that the height of maximum southerly winds associated with a gulf surge examined during SWAMP 1990 increased from north to south (Stensrud et al. 1997). Even though the flow is weaker along the southern gulf compared to the north on 13 July, a similar wind structure generally emerges from the results of this study (Figs. 4a, 5a, and 6a). The differences in the strength of the flow from north to south may in part be explained by the fact that the timing of the surge in the north is coincident with the GoC nocturnal low-level jet (LLJ) (Douglas 1995; Douglas et al. 1998), leading to amplification of the flow. This LLJ was present ~75% of the mornings at Yuma during SWAMP 1990 with the strongest winds located between 300-600 m and maximum speeds reaching 20 m s^{-1} (Douglas 1995) peaking at 0100 LT along the GoC east coast (Douglas et al. 1998). These results indicate that the gulf surge likely traversed the length of the GoC and first passed Los Mochis around 0000 UTC 13 July. Its structure varied from south to north, with the flow being stronger and shallower in the north, consistent with the WP-3D aircraft observations on 13 July (Higgins et al. 2006) and previous studies (Stensrud et al. 1997).

The time series of surface observations at Los Mochis (Fig. 6b) indicate a similar substantial increase in the surface pressure (~9 hPa) over a two-day period. However, there was no significant trend in the surface temperature or dewpoint during this time. Los Mochis' inland location may have limited the cooling observed at this site.

Given the continuity of surface pressure increases at the ISS sites, maps of surface pressure anomalies were constructed using data from the WMO METAR, ISS, and SMN automated sites

to track the regional impacts of the surge on the surface pressure field (Fig. 7). Data shown are 25-h running mean surface pressure anomalies (from 7 July to 14 August means) every six hours interpolated onto a regular 1°x1° grid over the core NAM region. Anomalies were investigated because some sites reported sea-level pressure and others reported station pressure. Twenty-five-hour running means were used to smooth the data and remove the diurnal and semidiurnal tidal signals.

At 0000 UTC 13 July (Fig. 7), the region surrounding the GoC was dominated by negative surface pressure anomalies. However, at this time the -1 hPa isobar exhibits an arc shape between the coasts of the southern GoC. Subsequently, this arc-shaped feature propagates northwestward along the axis of the GoC, such that by 1800 UTC 13 July, positive surface pressure anomalies replaced negative values along the majority of the GoC and its coastal plain. This pattern agrees qualitatively well with a similar surge-related surface pressure analysis conducted by Douglas and Leal (2003) using nine years of NCEP reanalyses data. By 0000 UTC 14 July, a large area of surface pressure anomalies greater than +1 hPa was located over the northern GoC. This maximum strengthened significantly over the following 24 hours (not shown) such that by 0000 UTC 15 July, areas over the Sonoran Desert had surface pressure anomalies of +4 hPa or more. These continued pressure rises are most likely related to the propagation of TS Blas (Figs. 2a and 3).

b.) Vertical Structure as Observed by Rawinsondes

To further explore the properties of the surge along the GoC, time series have been created from the four or six-hourly sounding data. Fields of potential temperature and moisture flux (meridional wind multiplied by mixing ratio) anomalies from 5 July to 15 August means were computed from 1000 to 500 hPa at six sites (Yuma, Puerto Peñasco, Bahia Kino, Empalme, Los

Mochis, and Mazatlan) for the period 0000 UTC 11 July to 0000 UTC 16 July (Fig. 8). Anomalies were calculated in such a way as to remove the diurnal tidal signal. Interpolation was conducted over data points flagged as bad or questionable from the quality control procedure and a 1-2-1 filter was applied in the vertical to smooth high frequency noise.

Warming below 600 hPa was observed at each site prior to gulf surge onset (Figs. 8a-f). This warming was especially strong nearer the surface and along the northern GoC (+2 to +6 K). Similar warming signatures at Los Mochis (Fig. 8e) and Mazatlan (Fig. 8f) were less extensive and generally weaker. This overall pattern agrees well with the composite results of Douglas and Leal (2003). They show anomalous warming of +2.5°C peaking one day prior to gulf surge onset around 950 hPa at Empalme.

This pattern was abruptly interrupted by gulf surge onset during the early morning hours on 13 July. Onset is readily identified by the large maxima of positive moisture flux and associated cooling from Empalme north to Yuma. These changes were generally largest below 800 hPa, in agreement with Douglas and Leal (2003), and lasted for several hours. The greatest surge-related cooling (-2 to -4 K) and positive moisture flux (> +150 m g s^{-1} kg^{-1}) occurred at Puerto Peñasco and Bahia Kino, consistent with the stronger gulf surge wind profiler signatures at these sites (Figs. 4a and 5a). The weaker signal at Yuma can be related to the fact that gulf surge intensity weakens as it fans out over the low deserts of Arizona (Hales 1972; Brenner 1974). Relatively strong positive moisture flux occurred at Los Mochis from 1200 UTC 12 July to 1200 UTC 13 July, but unlike the sites farther north, the strongest cooling was elevated (near 700 hPa) as it was also at the RV *Altair* (not shown). However, the latter results cannot be generalized since the maximum cooling at Los Mochis for the surge on 22-24 July occurred nearer the surface (not shown). The elevated cooling signal (also visible at Empalme around 1200 UTC 13

July) may be associated with the northward advection of cool air from the tropical east Pacific Ocean via TS Blas. However, mid-tropospheric moistening and evaporational cooling from convection propagating off the SMO may have also contributed to this feature since it appears the cooling is generally not accompanied by maxima of positive moisture flux.

As TS Blas propagated northwest (Figs. 2a and 3), its associated cooling and positive moisture flux are seen at Bahia Kino northward by 1200 UTC 14 July as a distinct and separate feature from that of the initial gulf surge a day prior. Accompanied by relatively strong positive moisture flux at this time (> +50 m g s^{-1} kg^{-1}), strong cooling (-2 to -6 K) up to 700 hPa was observed. The positive moisture fluxes are due to the strong south-southeasterly flow on 14 July, visible in the profiler data at the northern ISS sites (Figs. 4a and 5a).

Given the difficulty of accurately defining gulf surge vertical structure along the southern GoC from the above methods, an along-gulf cross section (23°N,108°W to 32°N,115°W) (Fig. 1) showing along gulf component winds, mixing ratios, and potential temperatures was generated from the T1A gridded dataset every six hours on 13 July (Fig. 9). Although the cross section contains interpolated rawinsonde data using onshore observations (except at the RV *Altair*), areas along the southern GoC are better represented than those to the north given the five rawinsonde sites nearby (Fig. 1).

At 0000 UTC, the strongest winds were along the southern gulf above 900 hPa. The greatest moisture (> 12 g kg^{-1}) was within the lowest 100 hPa of the atmosphere and extended north to ~30°N. A significant dome of cold air resided below 800 hPa along the southern gulf, as evident in the sloping isentropes. A cold-air dome was also evident over the southern GoC and intersecting the SMO at this time when examining east-west cross sections (not shown). This cooler air is most likely associated with evaporational cooling from convection associated with

TS Blas and the developing convection along the SMO (Fig. 3). Six hours later (0600 UTC), the cold-air dome moved north ~2° latitude. Concurrently, a stable layer developed below 900 hPa along the northern GoC, as evident in the tightly packed isentropes, likely aided by nocturnal cooling aliased from coastal sites out over the water. The strongest winds were still along the southern gulf, although there was a slight amplification of the low-level flow throughout most of the gulf. Mixing ratios less than 12 g kg^{-1} continued to encompass most regions to the north.

Significant changes occurred by 1200 UTC. The cold-air dome advanced northward and appeared to have reached the low deserts of northwest Mexico as the 302 K isentrope now extended along the entire length of the GoC. The low-level stable layer appeared to have been lifted somewhat over the northern half of the gulf, although this feature is not well resolved by the analysis. Strong winds (> 10 m s^{-1}) and abundant moisture (> 16 g kg^{-1}) below 800 hPa were now over the northern gulf. These patterns qualitatively held through 1800 UTC, although moisture maxima decreased slightly. In addition, a cold-dome appeared to redevelop along the central gulf below 900 hPa in response to strong afternoon diurnal heating over the deserts surrounding northern regions.

c.) Horizontal Structure

The horizontal extent of the gulf surge is more difficult to resolve than the vertical due to the spacing of rawinsonde sites around the GoC. In particular, there were no upper-air observations along northern Baja California or over the northern/central GoC waters (Fig. 1). Pilot balloon observations were made along Baja California during the NAME field campaign, but were not available for this analysis. In attempt to define the horizontal extent, gridded data from the T1A domain were used to generate 925 hPa maps from 0000 UTC 13 July to 0000 UTC 14 July showing potential temperature and moisture flux anomalies (as in Fig. 8) from 7 July to 15

August means (Fig. 10). Again, anomalies were calculated in such a way as to remove the diurnal tidal signal. The 925 hPa level was used since this was the approximate pressure level where gulf surge cooling and positive moisture flux appeared strongest along the northern gulf (Fig. 8).

At 0000 UTC 13 July, the region surrounding the GoC was warm, except for moderate cooling (0 to -2 K) along the coastal plain centered near Los Mochis. Despite this, the beginnings of the gulf surge emerged near the mouth of the gulf, as evident in the positive moisture flux maximum. This latter feature strengthened and expanded such that by 0600 UTC, it was centered over the southern gulf and accompanied by slightly stronger cooling (-2 to -3 K). These patterns extended beyond the immediate confines of the gulf perhaps due to the relatively coarse horizontal resolution of the gridded dataset.

Six hours later (1200 UTC) the surge reached the northern gulf. Very strong cooling (-2 to -4 K) and positive moisture fluxes (> +100 m g s^{-1} kg^{-1}) were approximately centered about Bahia Kino. While the most prominent surge signatures were now nearer the east GoC coast, this result may be biased by the locations of the rawinsonde sites along the northern gulf (Fig. 1). In fact, NOAA WP-3D measurements along the northern GoC at ~1700 UTC 13 July suggest the greatest gulf surge-related moisture flux was located over the waters of the GoC below 900 hPa and not necessarily along the gulf's eastern shores (Higgins et al. 2006). Perhaps the surge signatures earlier in the day centered over the waters of the GoC reflect better data coverage along the southern gulf.

At 1800 UTC, the surge was confined over the northern gulf between Bahia Kino and Puerto Peñasco with continued strong cooling and positive moisture fluxes. Although these signals are still centered about the GoC east coast, they are also clearly detached from the cooling and

positive moisture flux now entering the southern gulf in association with TS Blas. As the gulf surge signatures waned by 0000 UTC 14 July along the northern gulf, the northwestward propagation of TS Blas was evident to the south. While the horizontal structure of the surge was primarily confined to the GoC and its coastal plain, future analyses of high resolution observations and/or mesoscale model runs must be conducted to verify this result.

5. Propagation Characteristics and Dynamical Mechanisms

Theories for gulf surges suggest they are either advective (gravity current, isallobaric flow) or propagating (Kelvin or Rossby wave) phenomena (Zehnder 2004). The complexity of flows associated with the 13-14 July surge as well as limitations in the NAME observational network precludes a thorough analysis of surge dynamics. However, the bulk of evidence does suggest that this particular surge event was a propagating phenomenon. In particular, if we first examine the wind-speed maxima at the three ISS sites, their centroids may be tracked to give a propagation speed for this feature.

To do this, it is advantageous to show ISS profiler and surface winds at their full half-hour time resolution from 1800 UTC 12 July to 0000 UTC 14 July up to 2 km (Fig. 11). To best investigate surge behavior and dynamical mechanisms, also shown are ISS linearly interpolated sounding potential temperature anomalies from 5 July to 15 August means (as in Fig. 8), and surface pressure and temperature anomalies (from 7 July to 14 August means). The anomalies presented here should depict true meteorological signals, as the diurnal tide has been removed.

The initial gulf surge-related wind-speed maxima are centered near 0300 UTC at Los Mochis (Fig. 11c), 1000 UTC at Bahia Kino (Fig. 11b), and 1400 UTC at Puerto Peñasco (Fig. 11a), which yield (assuming the disturbance is channeled along the axis of the gulf) propagation speeds of ~17 m s^{-1} between Los Mochis and Bahia Kino and ~22 m s^{-1} between Bahia Kino and

Puerto Peñasco. These speeds exceed most of the flow speeds in the lower troposphere throughout the period, suggesting the surge is indeed a propagating phenomenon.

The cold-air intrusion depicted in Fig. 9 and seen in Fig. 10 initially in the south is likely due to strong evaporational cooling from deep convection (Fig. 3). These findings suggest that the gulf surge may have first initiated as a barrier-induced linear Kelvin wave-like disturbance (Reason and Steyn 1992; Skamarock et al. 1999; Zehnder 2004). However, the calculated gulf surge propagation speed (~17-22 m s^{-1}) is too fast for a pure linear Kelvin wave (~10 m s^{-1} or less) (Ralph et al. 2000). Speeds of ~20 m s^{-1} seem to fall more in line with nonlinear wave phenomena, such as atmospheric bores (Simpson 1997), which have been found to propagate at speeds greater than 15.0 m s^{-1} across portions of Oklahoma (Fulton et al. 1990) and the mid-Atlantic States (Koch et al. 1991). However, there is also the possibility that the surge behaves like a mixed-Kelvin wave bore, as has been found for coastally trapped wind reversals along the California coast (Ralph et al. 2000).

Bores are generally shallow-water disturbances that propagate along the tops of low-level stable layers and resemble a hydraulic jump, in which fluid depth significantly increases after passage (Simpson 1997). The fact that the surge arrived during the nighttime hours (particularly over the northern gulf) following the development of a nocturnal inversion raises the possibility that at least the initial surge impulse was a bore-like disturbance.

Boundary layer observations at Puerto Peñasco (Fig. 12) indicate low-level inversions at 0000 and 0600 UTC 13 July. Downdraft outflows from convection (Fig. 3) impinging on this low-level stable layer would be capable of lifting it and creating a bore. In fact, the multiple convective systems in the region (Fig. 3) may have contributed to several bores over the area, much as has been observed at night during the recent International H_2O Project (IHOP)

(Weckwerth et al. 2004). The shelf-like layer of cooling just below 500 m at Bahia Kino and Puerto Peñasco in Fig. 11 may be evidence of bore-related cooling. Further evidence of bore-like behavior is the rapid rise of the surface pressure to a new level, especially at Puerto Peñasco (Fig. 11a) and Bahia Kino (Fig. 11b), which is a characteristic feature of bores (Simpson 1997). Following this initial impulse there is a deeper layer of cooling that extends to the surface and strong (up to 20 m s^{-1}) south-southeasterly winds, which may be related to a Kelvin wave. The Puerto Peñasco potential temperature and specific humidity profiles at 1200 and 1800 UTC (Fig. 12) indicate a deepening mixed layer accompanying this feature as the strong winds and turbulence extend the boundary layer upward. Another indication of a bore-like disturbance is that the surface temperatures at Puerto Peñasco and Bahia Kino (Figs. 11a and b) did not fall with passage of the disturbance. Instead, they rose slightly and only fell later with the presumed Kelvin wave disturbance. The slight warming may have been a result of downward mixing of warming air at night and/or temporary horizontal advection of warmer air from the GoC.

Similar surge-related features at Puerto Peñasco and Bahia Kino are not as evident at Los Mochis (Fig. 11c). The strong cooling (-3 to -4 K) below 500 m from 0400 to 1600 UTC 13 July is related to the intense convective outflow that passed the site near 0400 UTC. However, the moderate cooling (-1 to -3 K) and south-southeasterly flow (up to 10 m s^{-1}) from 500 m up to 2.0 km at this time is likely due to surge passage. This overall surge signature did not last long and was interrupted around 1800 UTC by strong warming and an increased easterly component flow aloft, thus highlighting the importance of local effects and Los Mochis' more inland location.

The sequence of events occurring on 13-14 July is complex and subject to several possible interpretations. However, the weight of the evidence presented here suggests that the initial surge over the northern gulf may be due to bore-like disturbances (possibly containing a series of

waves) that owed their existence to convective downdrafts impinging on the nocturnal inversion over the region. Strong pressure rises to a new level accompanied the passage of these disturbances at Bahia Kino and Puerto Peñasco. Following these initial pulses, a deeper layer of sharp cooling and strong winds ensued, which likely represents a Kelvin wave that appeared to travel along the entire gulf. Pressures continued to rise as this feature passed. Another possibility is that the leading edge of this Kelvin wave steepened nonlinearly into a bore-like disturbance (Skamarock et al. 1999). The data are not adequate to delineate between these possible mechanisms.

6. Summary and Conclusions

Gulf surges are complex atmospheric phenomena, yet extremely important to the North American Monsoon (NAM) as they are often associated with northward horizontal transport of cool, moist air to the low deserts of the southwest United States and northwest Mexico, at times resulting in explosive convective development over this region. This study reports on high-resolution wind profiler, rawinsonde, and surface observations of a prominent gulf surge on 13-14 July during the 2004 North American Monsoon Experiment (NAME). The surge structure and properties have been defined in a detail heretofore not possible.

The 13-14 July gulf surge was strong and deep (up to ~800 hPa), resulting in the development of a large mesoscale convective system (MCS) over southern Arizona on 14 July. The initial surge quickly traversed the length of the Gulf of California (GoC) at speeds of ~17-22 m s^{-1}. However, it was stronger and shallower in the north than the south, perhaps due to its arrival in the north at the time of the GoC low-level jet (LLJ). Extensive convection along the Sierra Madre Occidental (SMO) and GoC coastal plain developed after 0000 UTC 13 July in response to easterly wave passage and possibly an upper-level inverted trough. This convection, in

conjunction with TS Blas, likely played an important role in gulf surge initiation due to strong evaporational cooling over the coastal plain and gulf itself.

Preceded by anomalous warming (+2 to +6 K) and a low-level nocturnal inversion along the northern GoC, the surge was first observed near the mouth of the gulf as a large low-level cold dome. As the disturbance moved north, a strong increase in south-southeasterly flow (up to 20 m s^{-1} near 750 m at Puerto Peñasco and 1.25 km at Bahia Kino), anomalous cooling (-1 to -4 K), and anomalous positive moisture flux (> +150 m g s^{-1} kg^{-1}) were observed along the northern gulf. These patterns lasted ~12-18 h, followed by a brief break and then a strong resurgence of anomalous cooling and southerly flow over a deeper layer associated with the passage of TS Blas on 14 July. Surface signals related to surge passage were relatively weak compared to those 1-2 km above the surface, with the exception of substantial increases in surface pressure, surface warming followed by moderate cooling, and a slight strengthening of the wind from the south-southeast. These characteristics were more difficult to discern along the southern gulf.

The horizontal extent of the gulf surge was difficult to resolve due to the few rawinsonde sites along the GoC coasts, especially in the north and along Baja California. Nevertheless, surge strength appeared to be greatest near the waters of the GoC and confined to the natural channel created by the surrounding terrain.

Inferences regarding the dynamics of the gulf surge are inclusive, but the data suggests that the stage of the surge not associated with the passage of TS Blas consisted of two parts. First, the surge likely originated from cooling by convective downdrafts impinging on the low-level nocturnal inversion over the region, advancing initially as a series of bores (particularly in the north), and was amplified by the nocturnal LLJ in the north. Second, a Kelvin wave disturbance followed that appears to have propagated the length of the GoC. The leading edge of this Kelvin

wave may have also steepened nonlinearly into a bore-like disturbance, but this possibility cannot be resolved by the data. These features were accompanied by strong surface pressure rises to a new level and a deepening of the mixed layer along the northern gulf.

The results presented here reveal the complexity of the 13-14 July gulf surge and the environment in which it propagated. It is uncertain whether the observations can be applied in part or in whole to other gulf surge events. Future work should focus on further integrating other observational platforms from the 2004 NAME field campaign (i.e. aircraft, pilot balloon, radar, precipitation) into the gridded analyses as a means to more accurately compare against mesoscale model simulations. Only then can a more complete picture emerge concerning gulf surge structure and probable dynamical mechanisms.

7. Acknowledgements

This research has been supported by the National Science Foundation Mesoscale Dynamic Meteorology Program under Grant. No. ATM-0340602, the National Oceanic and Atmospheric Administration Office of Global Programs under Grant No. NA17RJ1228, and a one-year American Meteorological Society Graduate Fellowship. Special thanks are also in order for Paul Ciesielski and Brian McNoldy for their assistance throughout this project, and to Dan Lindsey for providing the satellite data.

REFERENCES

Adams, D. K., and A. C. Comrie, 1997: The North American Monsoon. *Bull. Amer. Meteor. Soc.,* **78,** 2197-2213.

Brenner, I. S., 1974: A surge of maritime tropical air – Gulf of California to the southwestern United States, *Mon. Wea. Rev.,* **102,** 375-389.

Bryson, R. A., and W. P. Lowry, 1955: Synoptic climatology of the Arizona summer precipitation singularity. *Bull. Amer. Meteor. Soc.,* **36,** 329-339.

Douglas, M. W., 1995: The summertime low-level jet over the Gulf of California, *Mon. Wea. Rev.,* **123,** 2334-2347.

_____, R. A. Maddox, K. Howard, and S. Reyes, 1993: The Mexican monsoon. *J. Climate,* **6,** 1665-1677.

_____, and S. Li, 1996: Diurnal variation of the lower-tropospheric flow over the Arizona low desert from SWAMP-1993 observations, *Mon. Wea. Rev.,* **124,** 1211-1224.

_____, A. Valdez-Mananilla, and R G. Cueto, 1998: Diurnal variation and horizontal extent of the low-level jet over the northern Gulf of California, *Mon. Wea. Rev.,* **126,** 2017-2025.

_____, and J. C. Leal, 2003: Summertime surges over the Gulf of California: Aspects of their climatology, mean structure, and evolution from radiosonde, NCEP reanalysis, and rainfall data, *Wea. Forecasting,* **18,** 55-74.

Fuller, R. D., and D. J. Stensrud, 2000: The relationship between tropical easterly waves and surges over the Gulf of California during the North American Monsoon, *Mon. Wea. Rev.,* **128,** 2983-2989.

Fulton, R., D. S. Zrnić, and R. J. Doviak, 1990: Initiation of a solitary wave family in the demise of a nocturnal thunderstorm density current, *J. Atmos. Sci.,* **47,** 319-337.

Hales, J. E. Jr., 1972: Surges of maritime tropical air northward over the Gulf of California, *Mon. Wea. Rev.,* **100,** 298-306.

Higgins, R. W., W. Shi, and C. Hain, 2004: Relationships between Gulf of California moisture surges and precipitation in the southwestern United States, *J. Climate,* **17,** 2983-2997.

_____, and W. Shi, 2005: Relationships between Gulf of California moisture surges and tropical cyclones in the eastern Pacific basin, *J. Climate,* **18,** 4601-4620.

_____, and Coauthors, 2006: The North American Monsoon Experiment (NAME) 2004 field campaign and modeling strategy, *Bull. Amer. Meteor. Soc.,* **87,** 79-94.

Howard, K. W., and R. A. Maddox, 1988: Mexican mesoscale convective systems - large-scale environmental conditions. Preprints, *III InterAmerican and Mexican Congress of Meteorology,* Mexico City, Mexico, 395-399.

Johnson, R. H., P. E. Ciesielski, B. D. McNoldy, P. J. Rogers, and R. K. Taft, 2006: Multiscale flow variability during the North American Monsoon Experiment, *J. Climate,* accepted, pending revisions.

Jurwitz, L. R., 1953: Arizona's two-season rainfall pattern, *Weatherwise,* **6,** 96-99.

Kalnay, E., and Coauthors, 1996: The NCEP/NCAR 40-year reanalysis project, *Bull. Meteor. Soc.,* **77,** 437-471.

Koch, S. E., P. B. Dorian, R. Ferrare, S. H. Melfi, W. C. Skillman, and D. Whiteman, 1991: Structure of an internal bore and dissipating gravity current as revealed by raman lidar, *Mon. Wea. Rev.,* **119,** 857-887.

Loehrer, S. M., T. A. Edmands, and J. A. Moore, 1996: TOGA COARE upper-air sounding data archive: development and quality control procedures, *Bull. Amer. Meteor. Soc.,* **77,** 2651-2671.

McCollum, D. M., R. A. Maddox, and K. W. Howard, 1995: Case study of severe mesoscale convective system in central Arizona, *Wea. Forecasting,* **10,** 643-665.

Nuss, W.A., D. W. Titley, 1994: Use of multiquadric interpolation for meteorological objective analysis, *Mon. Wea. Rev.,* **122,** 1611–1631.

Pytlak, E., M. Goering, and A. Bennett, 2005: Upper tropospheric troughs and their interaction with the North American Monsoon. Preprints, *19th Conf. on Hydrology, 85th Annual Amer. Meteor. Soc. Meeting,* San Diego, CA, Amer. Meteor. Soc., CD-ROM, JP2.3.

Ralph, F. M., P. J. Neiman, P. O. G. Persson, J. M. Bane, M. L. Cancillo, J. M. Wilczak, and W. Nuss, 2000: Kelvin waves and internal bores in the marine boundary layer inversion and the relationship to coastally trapped wind reversals, *Mon. Wea. Rev.,* **128,** 283-300.

Rasmusson, E. M., 1967: Atmospheric water vapor transport and the water balance of North America, *Mon. Wea. Rev.,* **95,** 403-426.

Reason, C. J. C., and D. G. Steyn, 1992: The dynamics of coastally trapped mesoscale ridges in the lower atmosphere, *J. Atmos. Sci.,* **49,** 1677-1692.

Reitan, C. H., 1957: The role of precipitable water vapor in Arizona's summer rains. Tech. Rep. on the Meteorology and Climatology of Arid Regions 2, 21 pp.

Sellers, W. D, and R. H. Hill, 1974: *Arizona Climate 1931-1972,* 2d ed. The University of Arizona Press, 616 pp.

Simpson, J. E., 1997: *Gravity Currents in the Environment and the Laboratory.* 2d ed. Cambridge University Press, 244 pp.

Skamarock, W. C., R. Rotunno, and J. B. Klemp, 1999: Models of coastally trapped disturbances, *J. Atmos. Sci.,* **56,** 3349-3365.

Stensrud, D. J., R. L. Gall, and M. K. Nordquist, 1997: Surges over the Gulf of California during

the Mexican monsoon, *Mon. Wea. Rev.,* **125,** 417-437.

Wakimoto, R. M., 1982: The life cycle of thunderstorm gust fronts as viewed with Doppler radar and rawinsonde data, *Mon. Wea. Rev.,* **110,** 1060-1082.

Weckwerth, T. M., D. B. Parsons, S. E. Koch, J. A. Moore, M. A. LeMone, B. B. Demoz, C. Flamant, B. Geerts, J. Wang, and W. F. Feltz, 2004: An overview of the International H_2O Project (IHOP_2002) and some preliminary highlights, *Bull. Amer. Meteor. Soc.,* **85,** 253-277.

Zehnder, J. A., 2004: Dynamic mechanisms of the gulf surge, *J. Geophys. Res.,* **109,** 1-14.

Figure Captions

Figure 1. 2004 NAME EOP rawinsonde sites. Site symbol refers to number of rawinsonde launches per day during the EOP and nine IOPs. Heavy dashed curves outline T1A and T2A domains. The solid curve through the axis of the GoC identifies the locations of the vertical cross sections shown in Fig. 9. Shaded contours represent elevation above sea level (m).

Figure 2. T2A a) 700 and b) 200 hPa heights (10 m intervals) and wind vectors (m s^{-1}) at 1200 UTC from 12 July to 14 July 2004. High and low heights are respectively labeled 'H' and 'L'.

Figure 3. Infrared GOES-10 satellite imagery over the core NAM domain at a) 2346 UTC 12 July, b) 0600 UTC 13 July, c) 1200 UTC 13 July, and d) 1800 UTC 13 July 2004. Shaded contours represent cloud top temperatures (°C).

Figure 4. Puerto Peñasco a) wind profiler data and b) surface data from 0000 UTC 12 July to 0000 UTC 15 July. In a), wind speed (m s^{-1}) (shaded contours) is plotted every half-hour and wind barbs every two hours. One full barb equals 5 m s^{-1}. Only those times and heights are plotted where NIMA/NWCA confidence values are greater than or equal to 0.5. In b), surface temperature (°C) (solid), dewpoint temperature (°C) (dotted), and pressure (hPa) (dashed) are averaged over and plotted every half-hour.

Figure 5. Same as in Fig. 4, except at Bahia Kino.

Figure 6. Same as in Figs. 4 and 5, except at Los Mochis.

Figure 7. 25-h running mean surface pressure anomaly isobars (hPa) from 0000 UTC 13 July to 0000 UTC 14 July 2004. Anomalies are calculated using 7 July to 14 August

means. Dotted contours are negative and shaded contours are positive. Contours over the eastern Pacific Ocean have been omitted due to the lack of observational pressure data in this region. Squares denote NWS or SMN WMO sites, triangles denote SMN automated sites, and stars denote ISS sites.

Figure 8. Half-hour interpolated rawinsonde potential temperature and moisture flux anomalies at a) Yuma, b) Puerto Peñasco, c) Bahia Kino, d) Empalme, e) Los Mochis, and f) Mazatlan from 0000 UTC 11 July to 0000 UTC 16 July. Anomalies are calculated using 5 July to 15 August means. Colored contours represent potential temperature anomalies (K). Solid (dotted) thin black curves represent positive (negative) moisture flux anomalies (m g s^{-1} kg^{-1}). Thick solid black curve equals 0 m g s^{-1} kg^{-1}, with each successive contour at (±) 50 m g s^{-1} kg^{-1} intervals.

Figure 9. T1A potential temperatures (2 K intervals), mixing ratios (g kg^{-1}), and along gulf wind component (m s^{-1}) from 0000 UTC 13 July to 1800 UTC 13 July every six hours along a cross section through the GoC (see Fig. 1) from 23°N,108°W to 32°N,115°W.

Figure 10. T1A 925 hPa potential temperature and moisture flux anomalies from 0000 UTC 13 July to 0000 UTC 14 July every six hours. Anomalies are calculated using 7 July to 15 August means. Colored contours represent potential temperature anomalies (K). Solid (dotted) thin black curves represent positive (negative) moisture flux anomalies (m g s^{-1} kg^{-1}). Thick solid black curve equals 0 m g s^{-1} kg^{-1}, with each successive contour at (±) 25 m g s^{-1} kg^{-1} intervals. White regions represent areas below the surface and the ISS sites are denoted by stars.

Figure 11. Top panels depict half-hour interpolated rawinsonde potential temperature anomalies (K) (colored) at a) Puerto Peñasco, b) Bahia Kino, and c) Los Mochis from 1800 UTC 12 July to 0000 UTC 14 July. Also shown are profiler and surface wind data every half-hour. One full barb equals 5 m s^{-1} and the white contours highlight wind speed (m s^{-1}). Bottom panels depict surface pressure (hPa) (black) and temperature (°C) (red) anomalies every minute. See text for further details.

Figure 12. Puerto Peñasco rawinsonde potential temperature (solid) (K), specific humidity (dotted) (g kg^{-1}), and wind (1 full barb = 5 m s^{-1}) profiles at 0000, 0600, 1200, and 1800 UTC 13 July. Profile gaps are bad or questionable data as determined by the quality control.

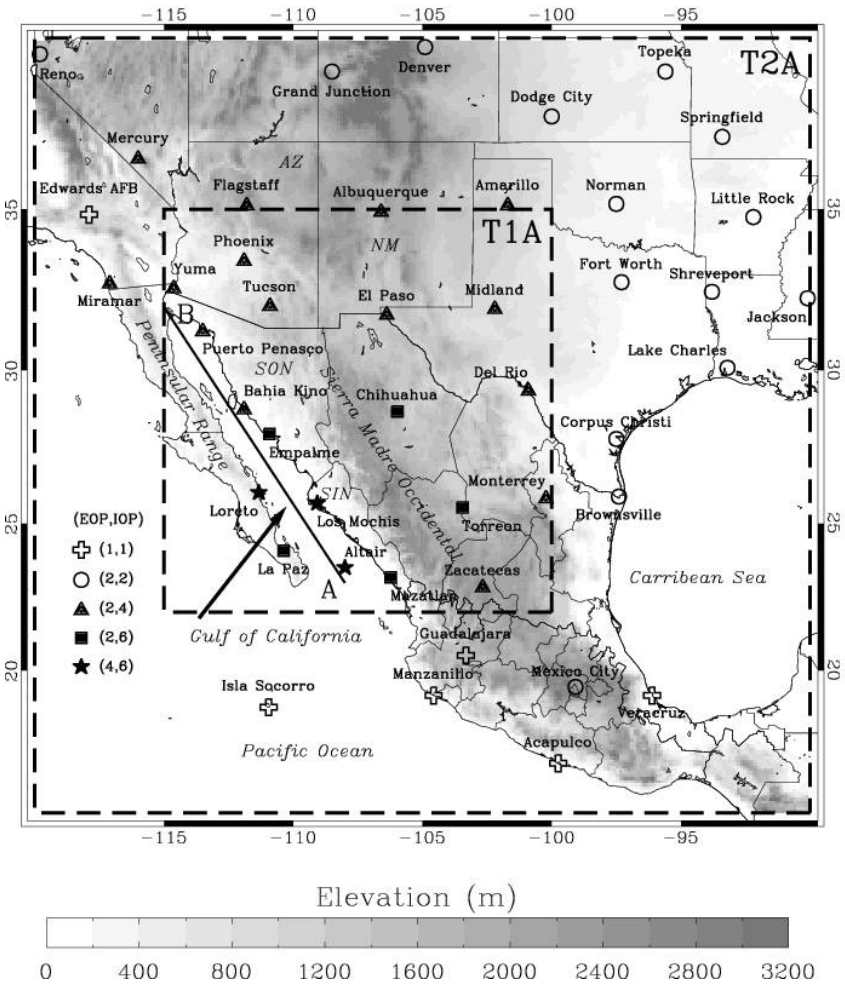

Figure 1: 2004 NAME EOP rawinsonde sites. Site symbol refers to number of rawinsonde launches per day during the EOP and nine IOPs. Heavy dashed curves outline T1A and T2A domains. The solid curve through the axis of the GoC identifies the locations of the vertical cross sections shown in Fig. 9. Shaded contours represent elevation above sea level (m).

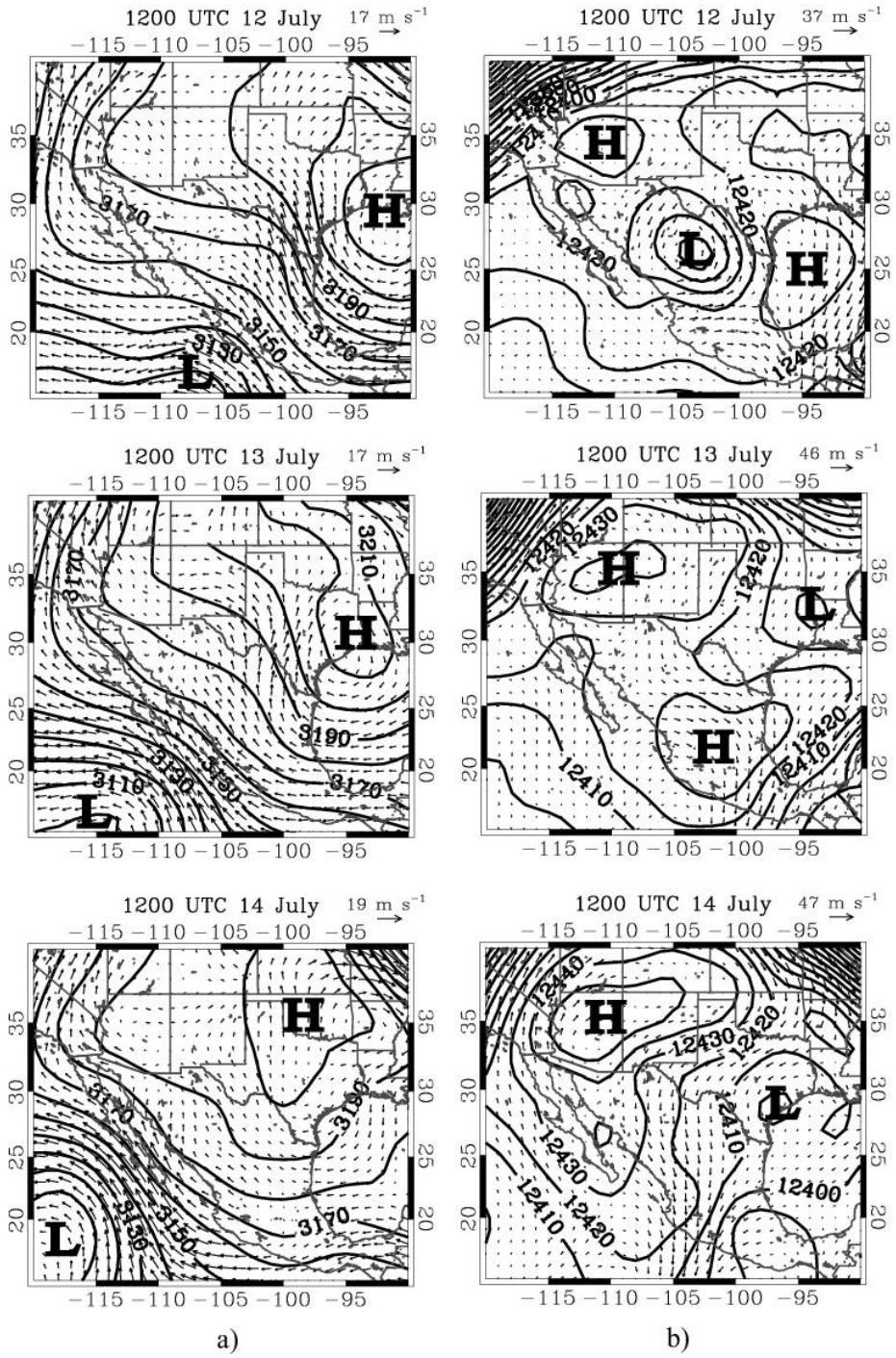

Figure 2: T2A a) 700 and b) 200 hPa heights (10 m intervals) and wind vectors (m s^{-1}) at 1200 UTC from 12 July to 14 July 2004. High and low heights are respectively labeled 'H' and 'L'.

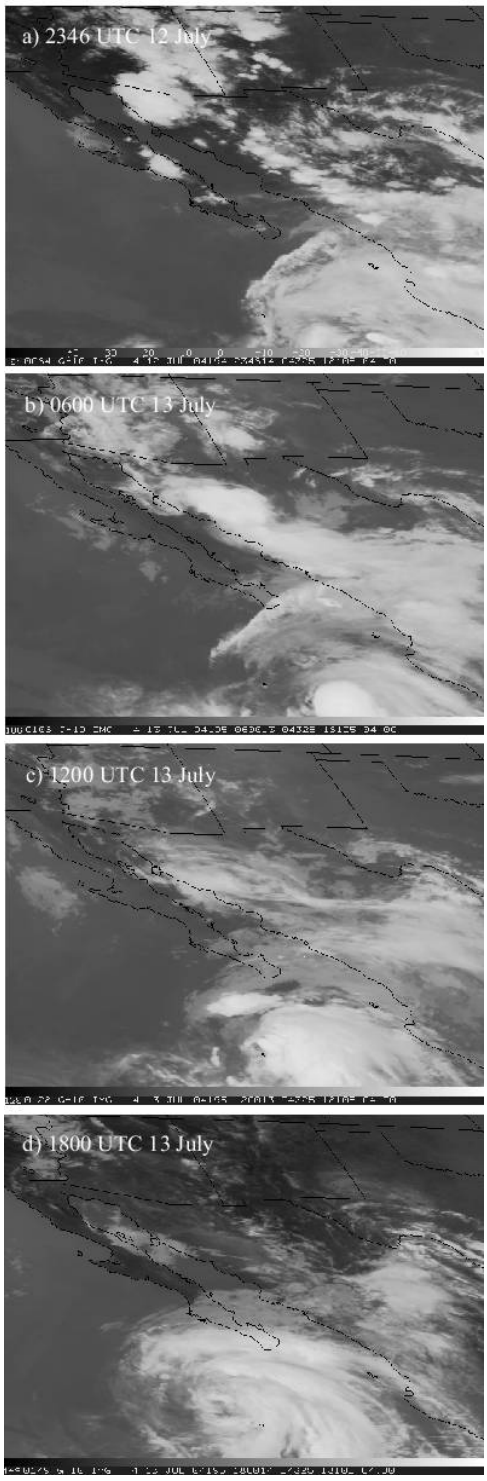

Figure 3: Infrared GOES-10 satellite imagery over the core NAM domain at a) 2346 UTC 12 July, b) 0600 UTC 13 July, c) 1200 UTC 13 July, and d) 1800 UTC 13 July 2004. Shaded contours represent cloud top temperatures (°C).

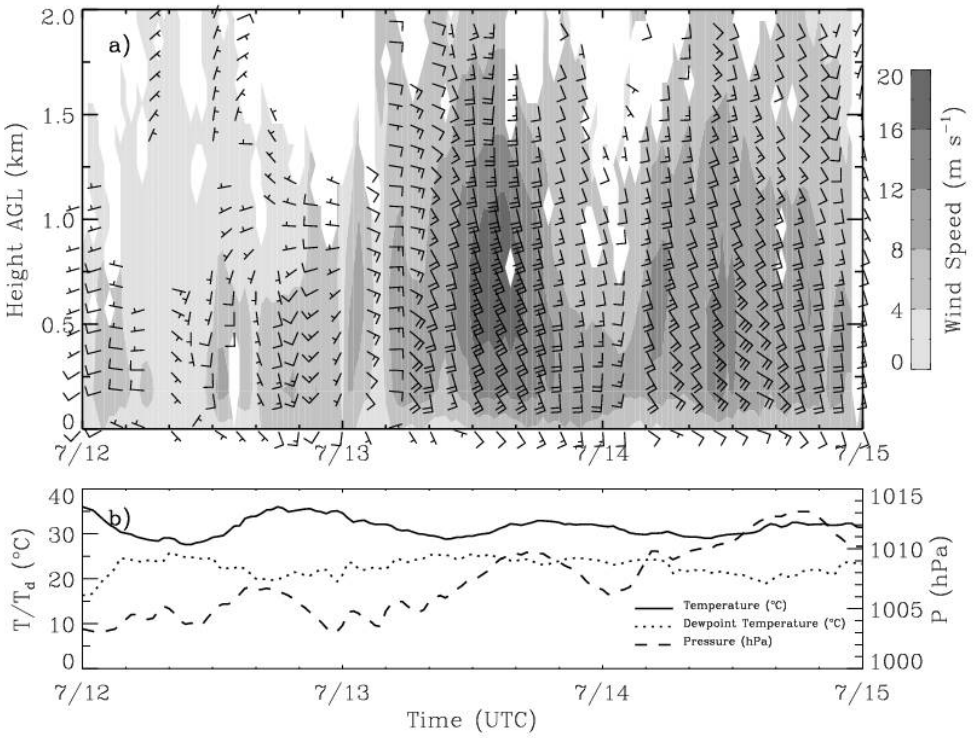

Figure 4: Puerto Peñasco a) wind profiler data and b) surface data from 0000 UTC 12 July to 0000 UTC 15 July. In a), wind speed (m s^{-1}) (shaded contours) is plotted every half-hour and wind barbs every two hours. One full barb equals 5 m s^{-1}. Only those times and heights are plotted where NIMA/NWCA confidence values are greater than or equal to 0.5. In b), surface temperature (°C) (solid), dewpoint temperature (°C) (dotted), and pressure (hPa) (dashed) are averaged over and plotted every half-hour.

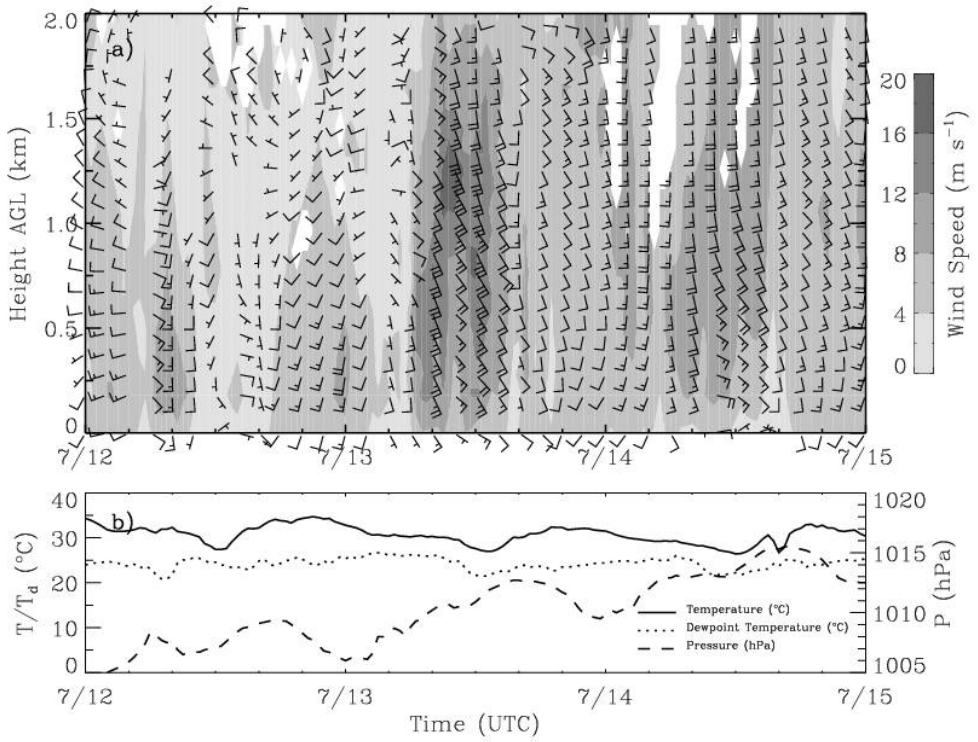

Figure 5: Same as in Fig. 4, except at Bahia Kino.

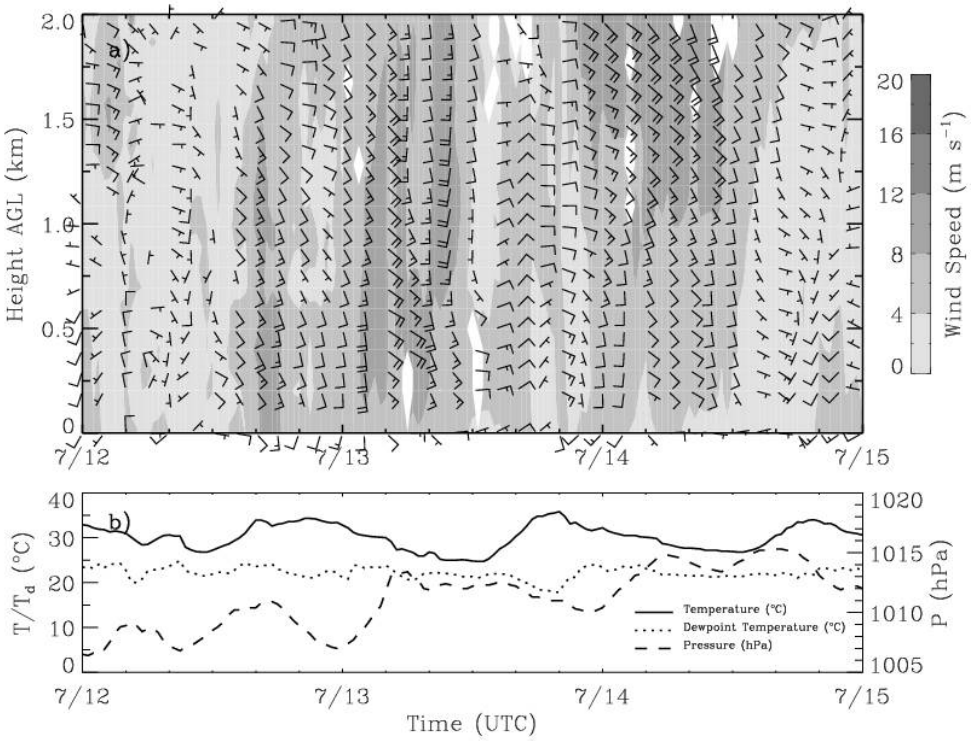

Figure 6: Same as in Figs. 4 and 5, except at Los Mochis.

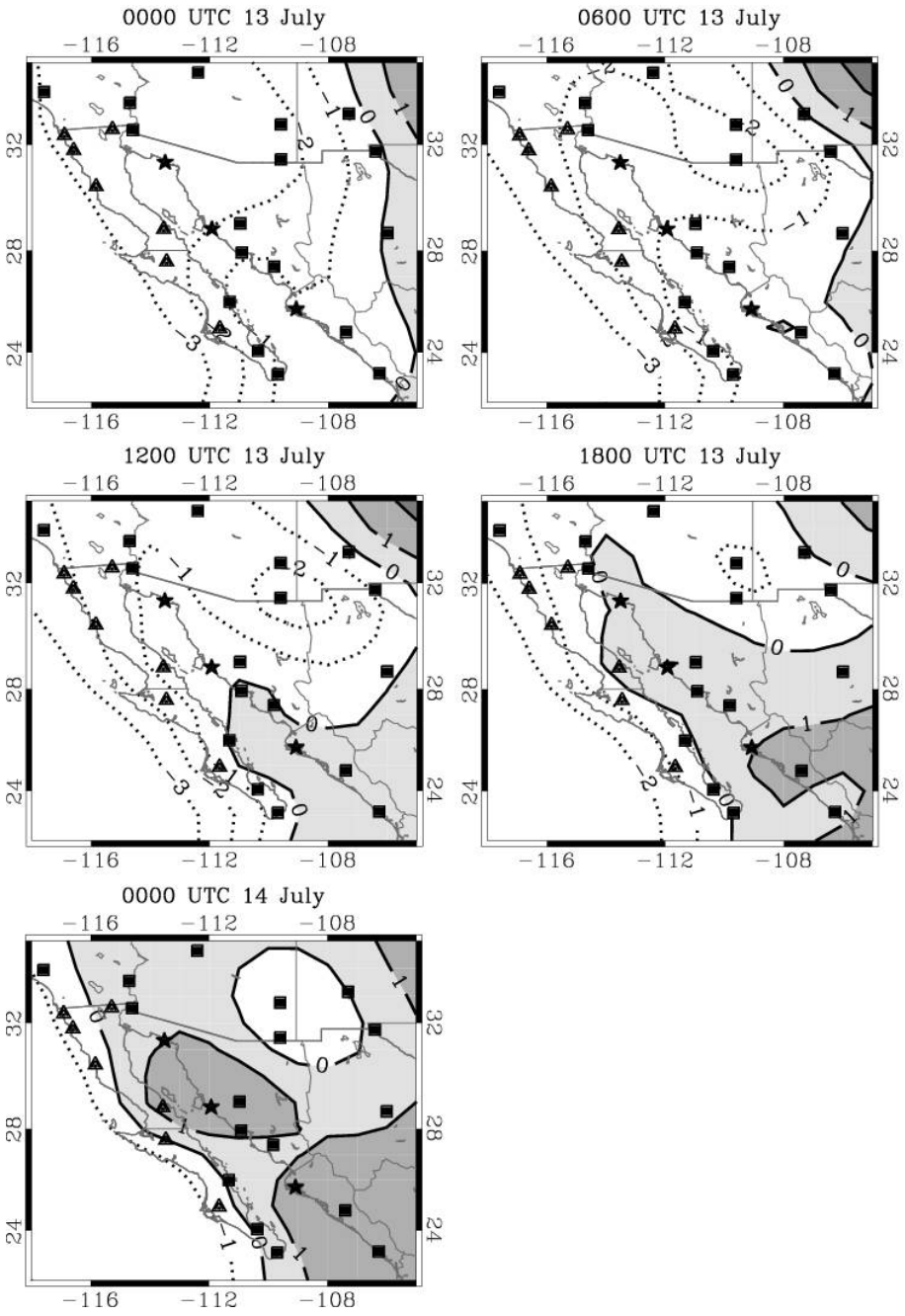

Figure 7: 25-h running mean surface pressure anomaly isobars (hPa) from 0000 UTC 13 July to 0000 UTC 14 July 2004. Anomalies are calculated using 7 July to 14 August means. Dotted contours are negative and shaded contours are positive. Contours over the eastern Pacific Ocean have been omitted due to the lack of observational pressure data in this region. Squares denote NWS or SMN WMO sites, triangles denote SMN automated sites, and stars denote ISS sites.

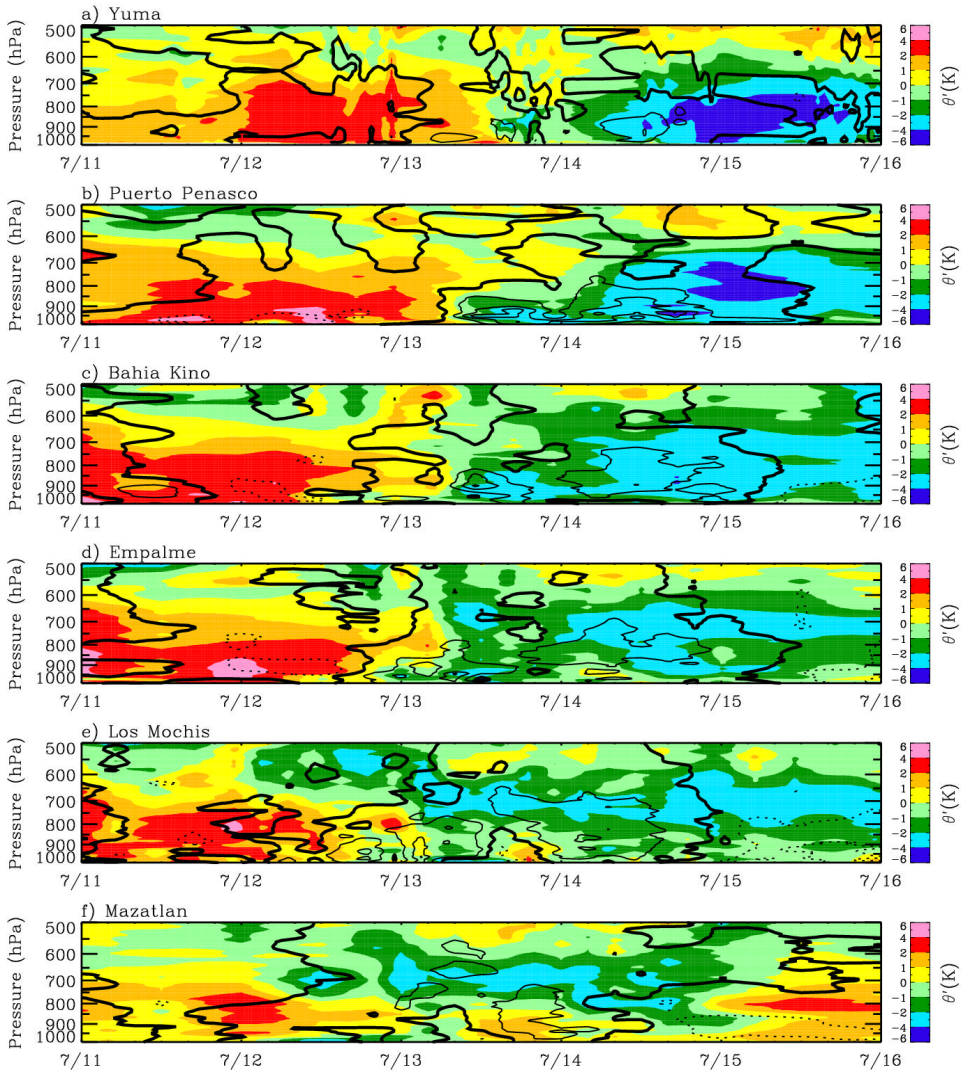

Figure 8: Half-hour interpolated rawinsonde potential temperature and moisture flux anomalies at a) Yuma, b) Puerto Peñasco, c) Bahia Kino, d) Empalme, e) Los Mochis, and f) Mazatlan from 0000 UTC 11 July to 0000 UTC 16 July. Anomalies are calculated using 5 July to 15 August means. Colored contours represent potential temperature anomalies (K). Solid (dotted) thin black curves represent positive (negative) moisture flux anomalies (m g s^{-1} kg^{-1}). Thick solid black curve equals 0 m g s^{-1} kg^{-1}, with each successive contour at (±) 50 m g s^{-1} kg^{-1} intervals.

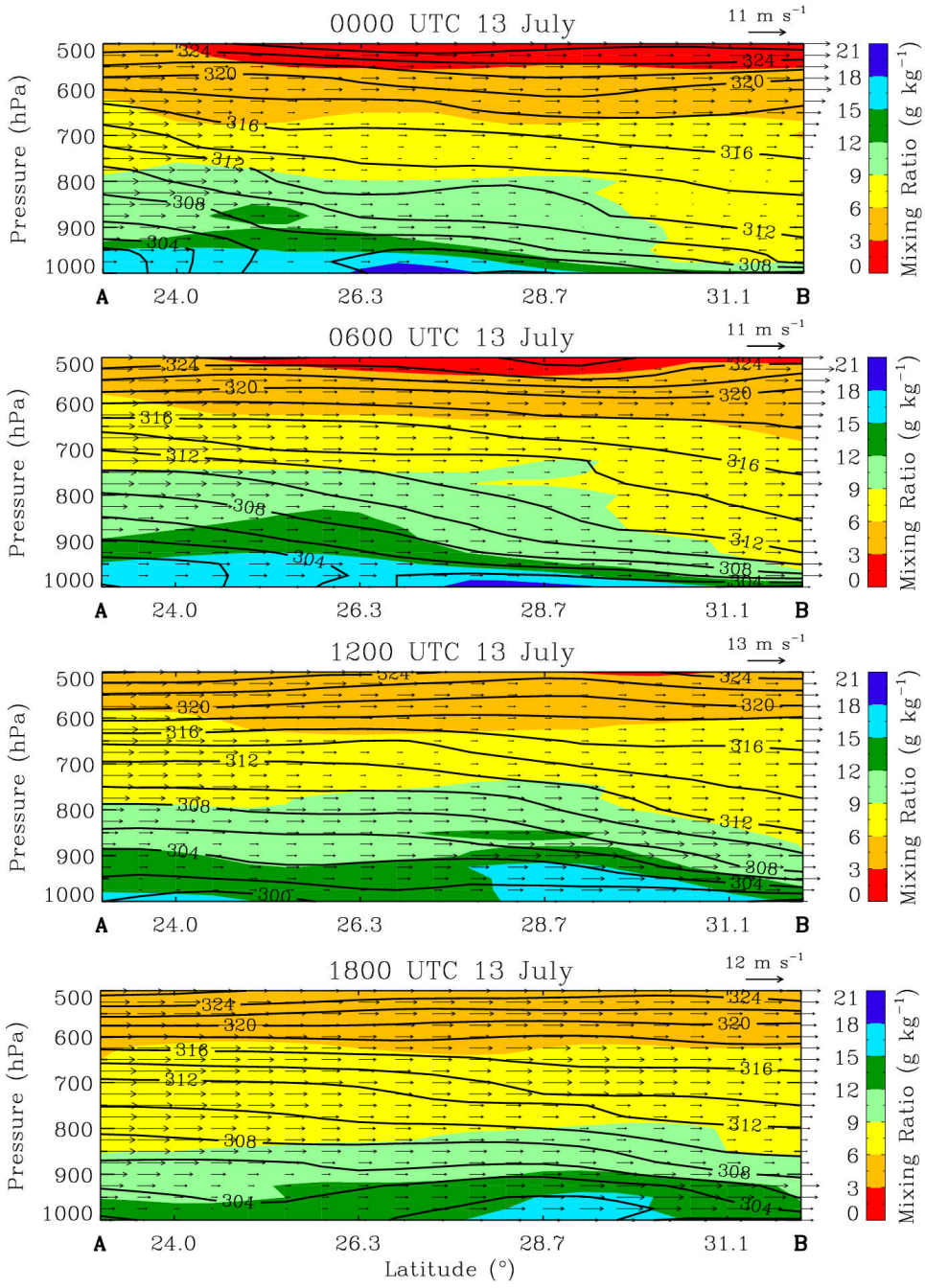

Figure 9: T1A potential temperatures (2 K intervals), mixing ratios (g kg^{-1}), and along gulf wind component (m s^{-1}) from 0000 UTC 13 July to 1800 UTC 13 July every six hours along a cross section through the GoC (see Fig. 1) from 23°N,108°W to 32°N,115°W.

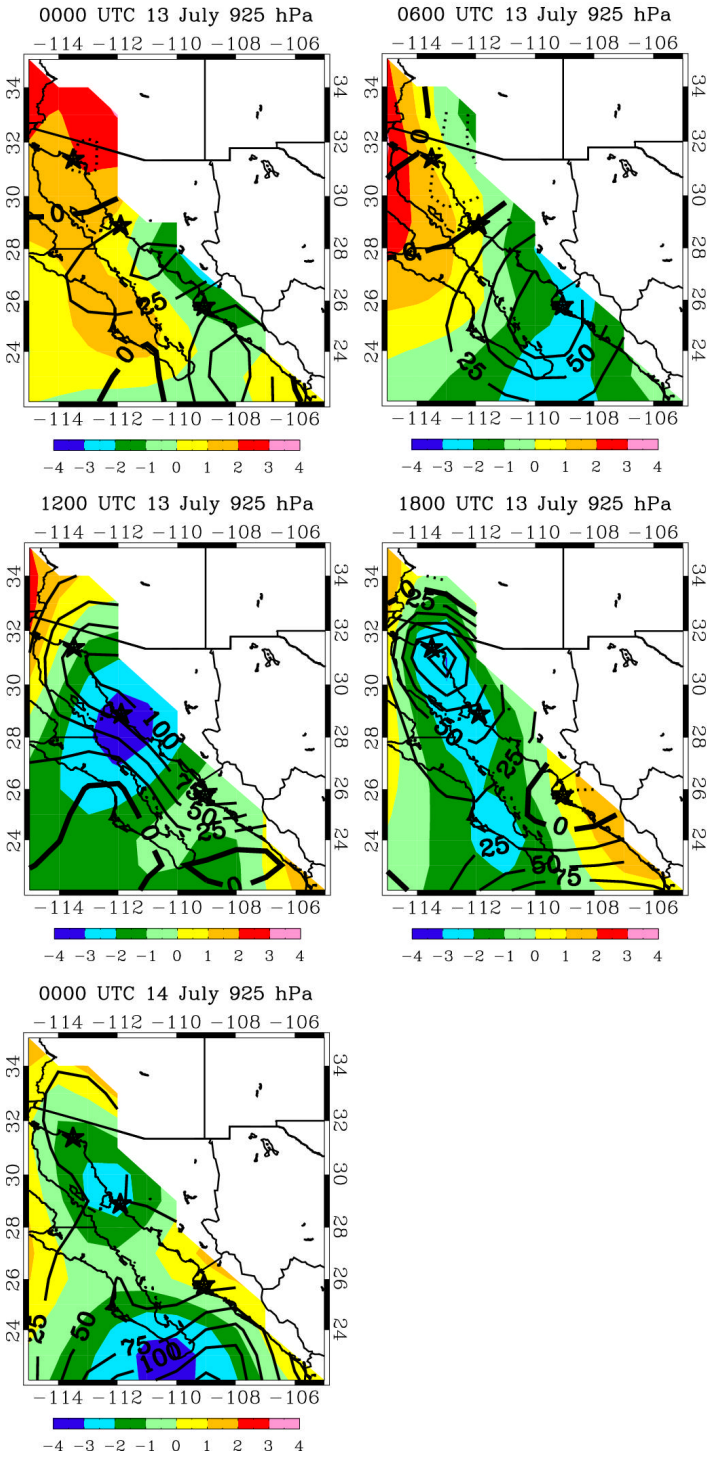

Figure 10: T1A 925 hPa potential temperature and moisture flux anomalies from 0000 UTC 13 July to 0000 UTC 14 July every six hours. Anomalies are calculated using 7 July to 15 August means. Colored contours represent potential temperature anomalies (K). Solid (dotted) thin black curves represent positive (negative) moisture flux anomalies (m g s^{-1} kg^{-1}). Thick solid black curve equals 0 m g s^{-1} kg^{-1}, with each successive contour at (±) 25 m g s^{-1} kg^{-1} intervals. White regions represent areas below the surface and the ISS sites are denoted by stars.

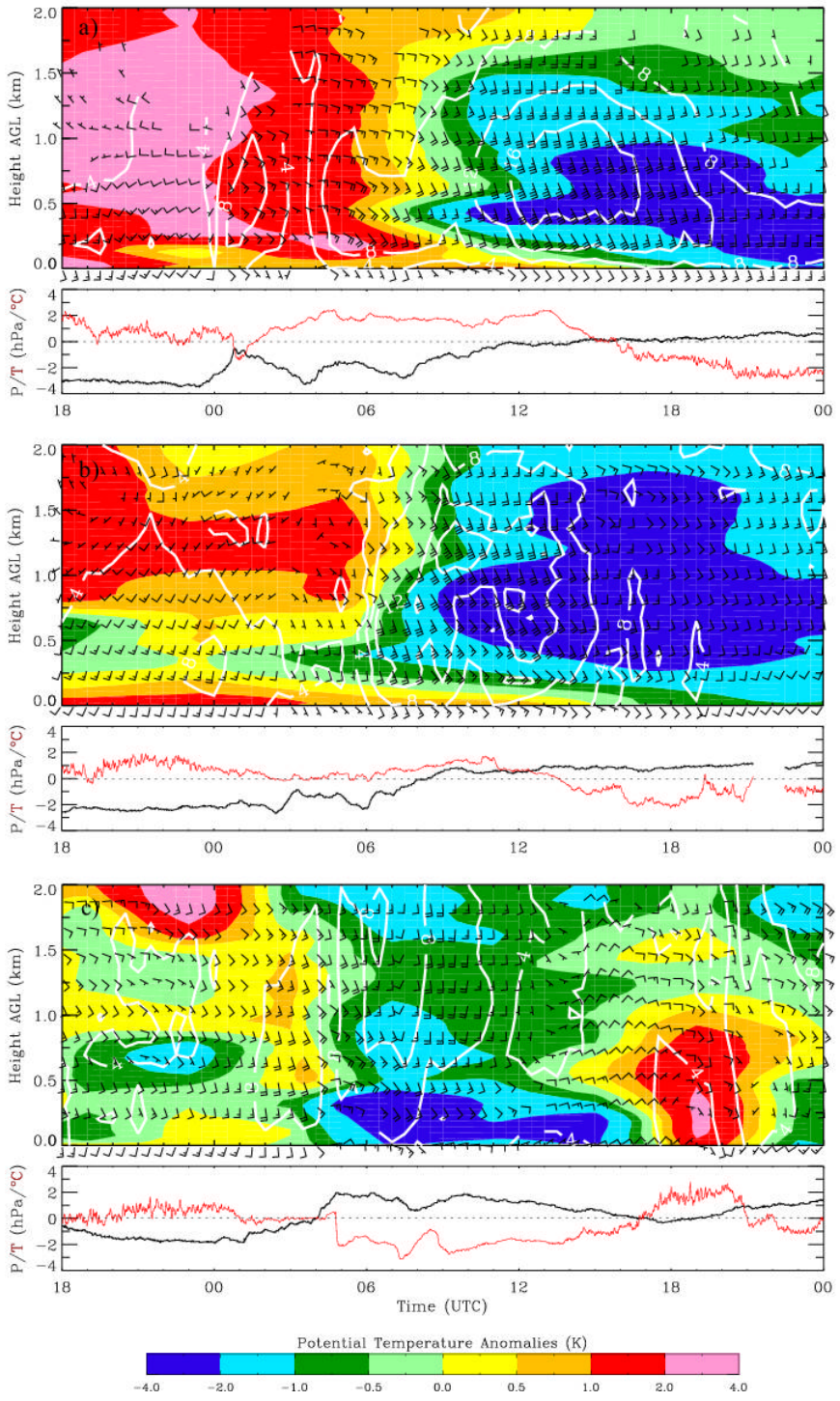

Figure 11: Top panels depict half-hour interpolated rawinsonde potential temperature anomalies (K) (colored) at a) Puerto Peñasco, b) Bahia Kino, and c) Los Mochis from 1800 UTC 12 July to 0000 UTC 14 July. Also shown are profiler and surface wind data every half-hour. One full barb equals 5 m s^{-1} and the white contours highlight wind speed (m s^{-1}). Bottom panels depict surface pressure (hPa) (black) and temperature (°C) (red) anomalies every minute. See text for further details.

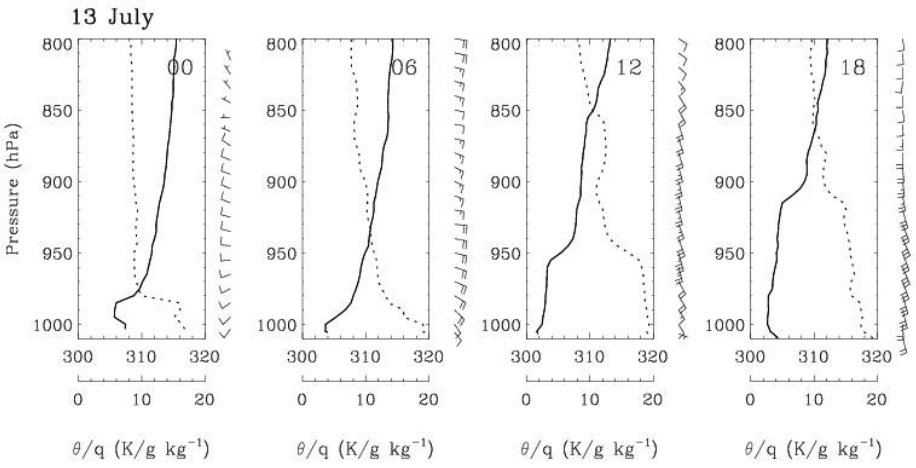

Figure 12: Puerto Peñasco rawinsonde potential temperature (solid) (K), specific humidity (dotted) (g kg^{-1}), and wind (1 full barb = 5 m s^{-1}) profiles at 0000, 0600, 1200, and 1800 UTC 13 July. Profile gaps are bad or questionable data as determined by the quality control.